



Ultrafast resonance energy transfer from a site-specifically attached fluorescent chromophore reveals the folding of the N-terminal domain of CP29

Bart van Oort^{a,*}, Sukumaran Murali^{a,1}, Emilie Wientjes^b, Rob B.M. Koehorst^{a,c}, Ruud B. Spruijt^a, Arie van Hoek^{a,c}, Roberta Croce^b, Herbert van Amerongen^{a,c}

^a Laboratory of Biophysics, Wageningen University, Dreijenlaan 3, 6703HA Wageningen, The Netherlands

^b Department of Biophysical Chemistry/Groningen Biotechnology and Biological Sciences Institute, University of Groningen, Nijenborgh 4, 9747 AG Groningen, The Netherlands

^c Microspectroscopy Centre Wageningen, Dreijenlaan 3, 6703HA Wageningen, The Netherlands

ARTICLE INFO

Article history:

Received 30 May 2008

Accepted 30 October 2008

Available online 17 November 2008

Keywords:

Lhcb4

FRET

Rhodamine

PSII

Photosystem II

Phosphorylation

npq

Photoprotection

ABSTRACT

The photosynthetic minor antenna complex CP29 of higher plants was singly mutated, overexpressed in *Escherichia coli*, selectively labeled with the fluorescent dye TAMRA at three positions in the N-terminal domain, and reconstituted with its natural pigments. Picosecond fluorescence experiments revealed rapid excitation energy transfer (~ 20 ps) from TAMRA covalently attached to a cysteine at either position 4 or 97 (near the beginning and end of the N-terminal domain) to the chlorophylls in the hydrophobic part of the protein. This indicates that the N-terminus is folded back on the hydrophobic core. In 20% of the complexes, efficient transfer was lacking, indicating that the N-terminus can adopt different conformations. Time-resolved polarized fluorescence measurements demonstrate that the non-transferring conformations only allow restricted rotational motion of the dye molecule. When TAMRA was attached to a cysteine at position 40, the overall transfer efficiency was far lower, reflecting a larger distance to the hydrophobic region.

© 2008 Elsevier B.V. All rights reserved.

1. Introduction

In higher plants sunlight is harvested by two multiprotein complexes, photosystem (PS) I and II and it is used to drive electron transfer reactions. The photosystems are composed of a core complex, which contains all the cofactors of the electron transport chain and of an external antenna, which harvests light and transfers excitation energy to the reaction centers. In photosystem II the antenna system consists of four complexes: LHClI, the major antenna subunit, present as a trimer in the membrane, and three minor monomeric complexes CP24, CP26 and CP29. The minor

complexes together contain 15% of the pigments of PSII and they are located between LHClI and the core proteins [1]. Besides playing a role in light harvesting they are also involved in photoprotective mechanisms (e.g. nonphotochemical quenching) that are used by plants to dissipate excess energy under high-light conditions [2–4]. It has been proposed that a change in structure of the minor complexes is responsible for a switch between the light-harvesting state and the quenching state [2].

Amongst the three minor complexes, CP29, the product of the *Lhcb4* gene, is the best characterized one. The spectroscopic properties of each pigment in each binding site have been determined with the help of mutation analysis followed by *in vitro* reconstitution [5–8] and by applying different spectroscopic techniques [9–12]. Several time-resolved studies have been performed on the complex, allowing to elucidate the energy transfer rates and pathways between Chls and between carotenoids and Chls [4,13–18]. CP29 is the largest of the outer antenna complexes of PSII and it is special because it contains an unusually long N-terminal domain (~ 100 amino acids). Under cold stress the N-terminus becomes phosphorylated at Thr83 [19] increasing the resistance of the plants to cold stress [20,21]. It was demonstrated that phosphorylation leads to a change in conformation of the protein [22], possibly favoring the dissipative form. More recently, a second phosphorylation site, corresponding to Thr6, was observed in the *Lhcb4.2* gene product [23]. Although the structure of CP29 has

Abbreviations: apo-4, apoprotein of mutant 4, labeled with TAMRA; Chl, chlorophyll; CP29, chlorophyll protein 29 (one of the minor antenna complexes of photosystem II); CP29-4, mutant 4, reconstituted with pigments, and labeled with TAMRA; CP29-40, mutant 40, reconstituted with pigments, and labeled with TAMRA; CP29-97, mutant 97, reconstituted with pigments, and labeled with TAMRA; CP29-WT, wild-type protein; DAS, decay-associated spectrum/spectra; DM, dodecyl β -D-maltoside; FRET, Förster resonance energy transfer; HPSEC, high performance size exclusion chromatography; LHClI, light-harvesting complex II; PSII, photosystem II; RC, reaction center; S/N, signal-to-noise ratio; TAMRA, 6-carboxy-tetramethyl-rhodamine; MTS-TAMRA, (2-((5(6)-tetramethylrhodamine)-carboxylamino)ethyl methanethiosulfonate).

* Corresponding author.

E-mail address: bartvoort@gmail.com (B. van Oort).

¹ Present address: Laboratory of Organic Chemistry, Wageningen University, Dreijenplein 8, 6703 HB Wageningen, The Netherlands.

not been resolved, the high sequence homology, especially in the transmembrane domain, suggests an organization similar to that of LHCII, the structure of which has been obtained at 2.5–2.72 Å [24,25]. However, no information is available about the organization of the N-terminal domain, which differs completely from that of LHCII.

The aim of the present work is to develop an alternative method to obtain structural and dynamical information on CP29 and in particular on its N-terminal domain. Mutagenesis techniques are used to produce single cysteine mutants at selected positions (4, 40 and 97) of the N-terminus. The mutated apoproteins were labeled with the fluorophore TAMRA, which can selectively be excited around 530–550 nm, and reconstituted with the natural pigments, chlorophylls *a* and *b* (Chl *a/b*) and carotenoids. In principle TAMRA might influence the protein's structure but the effect is probably minor because protein folding of the homologous protein LHCII is not affected by attachment of a similar label [26]. With the use of picosecond fluorescence techniques, resonance energy transfer (FRET) was measured from TAMRA to the Chl molecules, providing information about distances between specific sites of the N-terminal domain and the chlorophyll molecules.

2. Materials and methods

2.1. Construction and isolation of overexpressed CP29 apoprotein

Lhcb4.1 cDNA of *A. thaliana* (from Arabidopsis Biological Resource Center DNA Stock Center) was subcloned into a pT7-7 expression vector. The construct contains the sequence of the mature CP29 protein with an additional methionine at the N-terminus and a 6 His-tag at the C-terminus

Mutations were introduced using the Stratagene Quik Change Site Directed Mutagenesis Kit. First, the natural occurring cysteine (position 108) was replaced by alanine. On this template, cysteine mutations were introduced in the N-terminal peptide at positions 4, 40, and 97. The constructs were checked by DNA-sequencing. The plasmids were amplified in the super competent *Escherichia coli* XL-1 Blue strain and the proteins overexpressed in the *E. coli* BL21(DE3) strain [27,28].

2.2. Pigment isolation, labeling and reconstitution of CP29-pigment complexes

Purified pigments were obtained from spinach thylakoids. Concentrations of pigments were determined spectroscopically; Chls as described by Porra et al. [29] and Cars as described by Davies [30]. CP29 apoprotein mutants and wild-type were labeled with MTS-TAMRA, (2-((5(6)-tetramethylrhodamine)carboxylamino)ethyl methanethiosulfonate from TRC, Toronto, Canada), and purified from the excess of TAMRA using HPSEC and affinity chromatography on a His-Trap column [31]. Reconstitution and purification of protein-pigment complexes were performed as reported in [15]. The average labeling efficiency was $70 \pm 20\%$. Concentrated stock solutions of the CP29, containing dodecyl β -D-maltoside (DM; 0.06% W/V) and sucrose remaining from sucrose gradient purification, were diluted in sucrose-free DM buffer (0.06% W/V + 10 mM Na_2HPO_4 pH 7.6) for the fluorescence measurements.

2.3. Steady-state spectra

Steady-state absorption spectra were recorded on a Varian Cary 5E spectrophotometer. Steady-state fluorescence emission spectra (535 nm excitation) and steady-state fluorescence excitation spectra (680 nm detection) were recorded on a Spex-Fluorolog 3.2.2 spectrofluorimeter (Jobin-Yvon).

2.4. Time-resolved fluorescence using the streak-camera setup

For the picosecond fluorescence measurements excitation was performed with a set of lasers and optical amplifiers from Coherent Inc., Santa Clara, CA, USA. The output of a passively mode-locked titanium sapphire laser model Mira 900 (output wavelength 800 nm, average power 0.5 W, pulse width 130 fs, repetition rate 75.9 MHz) was used for seeding a regenerative amplifier model RegA 9000 (output wavelength 800 nm, average power 1.2 W, pulse width 130 fs, repetition rate 253 kHz). Continuous wave diode pumped solid-state Nd:YVO₄ lasers model Verdi V5 and Verdi V10 (wavelength 532 nm) were used for pumping the Mira and the RegA respectively. The output of the RegA fed an optical parametric amplifier (model OPA 9400). The average power output of the OPA was up to tens of mW at wavelengths ranging from 470 to 720 nm. Furthermore the frequency-doubled 800 nm light (400 nm), and a frequency doubler (APE GmbH, Berlin, Germany, model fs OPA-SHG) for the OPA output (then 210–360 nm wavelength) were available for excitation purposes. The light intensity was modulated with neutral density filters, and residual white light from the OPA was removed with an interference filter. The polarization was set vertical with a Berek polarizer (New Focus, San Jose, CA, USA model 5540), and further optimized using a Glan Taylor polarizer. A lens of 15 cm focal length then focused the light into the sample in a static fluorescence cuvette, resulting in a spot diameter of 150 μm . Care was taken to avoid internal reflections in the sample cells. In front of the streak-camera an imaging spectrograph was mounted (Chromex, Albuquerque, NM, USA model 250is). Fluorescence emission was collected from the sample cell and focused onto the input slit of the spectrograph using two identical achromatic lens assemblies (Sill Optics, Wendelstein, Germany, model UV APO special, $f = 70$ mm, $d = 22$ mm) placed in a complementary manner with a Glan Taylor polarizer (Leysop Ltd., Essex, England model GT20) and optionally an optical filter (to suppress scatter) in between. The polarizer was set at magic angle orientation. The spectrograph was equipped with a turret, carrying three gratings with different ruling and blaze wavelength. The output mirror of the spectrograph focused the output light directly onto the stripe-shaped (height 70 μm) cathode of the streak-camera (Hamamatsu Photonics K.K., Hamamatsu City, Japan model C5680 with model M5675 Synchroscan unit). Wavelength dispersion of the spectrograph was in a horizontal direction, the time dispersion of the streak tube was in a vertical direction. Four time windows are available for the streak camera: 160, 800, 1500 and 2100 ps. Scale, linearity and curving of the time and wavelength axes were extensively treated in correction procedures using the following references: Fabry-Perot etalons, fixed wavelength light sources and a white light source (Optronic Laboratories, Orlando, FL, USA model 65A ultra precise current source with model OL 220C 200W quartz halogen tungsten reference lamp). Spectral resolution is typically 2 nm, and temporal resolution ~ 1 ps. For more details on streak camera experiments and data analysis, see [32]. For the experiments described here the time window was 160 ps, and the spectral window ranged from 540 to 700 nm (using the grating with 50 grooves/mm ruling and 600 nm blaze).

2.5. Streak-camera data analysis

The streak-camera data were corrected for jitter if necessary, averaged, and background and shading corrected using the software package High Performance Digital Temporal Analyzer (HPDTA, version 6.4, Hamamatsu Photonics). The streak-camera images are two-dimensional data sets of fluorescence intensity as a function of time and wavelength. The images were sliced up into time traces of 6 nm width. These traces were fitted to a sum of exponentials using global analysis, with software described in

[33]. The resulting wavelength-dependent amplitudes provide the decay-associated spectra (DAS).

2.6. Time-correlated single photon counting

Time-correlated single photon counting was performed with a homebuilt setup, as described in [34]. Samples, placed in a static cuvette holder and maintained at 283 K, were excited with vertically polarized 540 nm pulses of around 0.2 ps duration at a repetition rate of 3.8 MHz, and measurements were done by collecting repeated sequences of 10 s vertically (parallel) and 10 s horizontal (perpendicular) polarized fluorescence emission. Fluorescence was collected through a Schott OG570 long pass filter, in combination with either a Schott IL585.1 interference filter (TAMRA fluorescence) or a Balzers 679 nm interference filter (Chl fluorescence). The excitation density was reduced to obtain a count-rate below 30,000 per second (sub-pJ pulse energy) and care was taken to minimize data distortion [35]. Data were acquired until the number of counts in the peak channel was $\sim 15,000$. The instrument response function (~ 50 ps FWHM) was obtained at 585 nm with erythrosine B in water (80 ps fluorescence lifetime [36]), and at 679 nm with pinacyanol iodide in methanol (6 ps fluorescence lifetime [37]). Data were corrected for background signal (less than 1%) by subtracting the signal of DM buffer measured directly after the sample.

Individual photons were detected by a microchannel plate photomultiplier, and arrival times were stored in 4096 channels (5 ps channel width) of a multichannel analyzer. Isotropic fluorescence decay curves $F_{iso}(t)$ were calculated from the decay curves of parallelly $F_{||}(t)$ and perpendicularly $F_{\perp}(t)$ polarized emission: $F_{iso}(t) = F_{||}(t) + 2gF_{\perp}(t)$, using the relative sensitivity g of the detection branch for parallelly and perpendicularly polarized light (g equals unity for this setup [38]). $F_{iso}(t)$ was fitted to a sum of exponentials, convoluted with the instrument response function [39]. Time resolved anisotropy was analyzed by global fitting of $F_{||}(t)$ and $F_{\perp}(t)$, with fit parameters τ_j (fluorescence lifetimes), a_j (fluorescence decay amplitudes), ϕ_k (anisotropy correlation times), β_k (anisotropy amplitudes) and β_{inf} (residual anisotropy), using fit functions $I_{||}(t) = \frac{1}{3} \sum_j a_j e^{-t/\tau_j} * (1 + 2(\beta_{inf} + \sum_k \beta_k e^{-t/\phi_k}))$ and $I_{\perp}(t) = \frac{1}{3} \sum_j a_j e^{-t/\tau_j} * (1 - (\beta_{inf} + \sum_k \beta_k e^{-t/\phi_k}))$, convoluted with the instrument response function, as described in detail by Visser et al. [40]. The quality of a fit was judged by the χ^2 value and by the quality of residuals and autocorrelation thereof.

3. Results

The naturally occurring cysteine (position 108) was replaced by alanine, and single-point mutations were introduced in the N-terminal loop of CP29 at three different positions. In the three mutated proteins, a cysteine replaced the wild-type amino acids at positions 4, 40 and 97, respectively (see also Fig. 1) and this cysteine was labeled with TAMRA with an average efficiency of $70 \pm 20\%$. For all complexes, absorption and steady-state excitation and emission spectra were measured as well as time-resolved fluorescence kinetics upon excitation in the TAMRA absorption region. Below the results on labeled CP29 mutated at position 4 (CP29-4) will first be presented in detail. The data analysis of the other complexes was done in an analogous way and the results will be summarized afterwards.

3.1. Absorption

The absorption spectra of wild-type CP29 (CP29-WT) and labeled CP29-4 are given in Fig. 2A. The spectra are nearly identical over the entire wavelength range with the exception of the region around 550 nm, where the labeled protein shows the additional

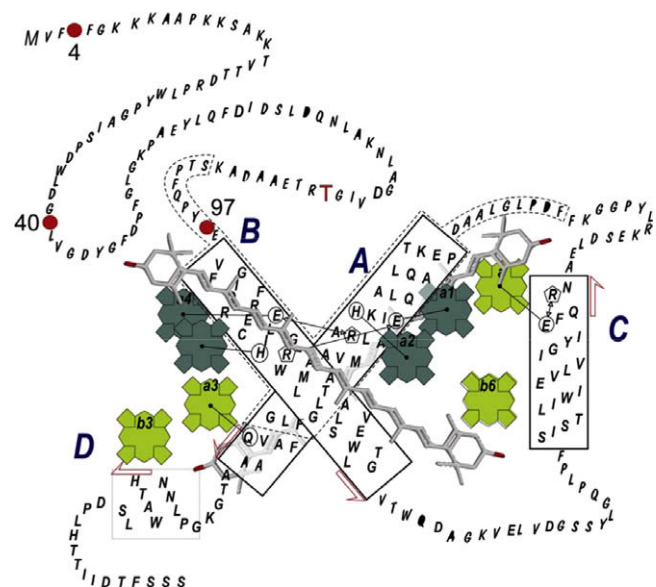


Fig. 1. Schematic representation of the structure of CP29 (sequence of *Lhcb4.1* of *Arabidopsis thaliana*) with positions of Chl *a* (dark green), positions where Chl *a* or *b* bind (light green) and the two central carotenoids (grey) [5]. The red dots and numbers indicate the position of the labeled residues used in this work. The red T indicates the site of phosphorylation [19]. (For interpretation of the references to colour in this figure legend, the reader is referred to the web version of this article.)

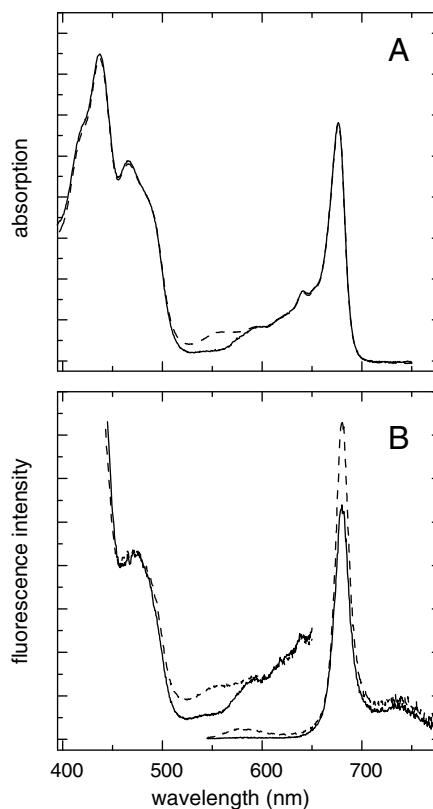


Fig. 2. Steady-state spectra of CP29-WT (solid) and CP29-4 (dashed). (A) Absorption spectra normalized at 676 nm. (B) Fluorescence emission (right, excitation at 535 nm) and excitation (left, detection at 680 nm) spectra normalized to the Chl concentration.

absorption of TAMRA. For the time-resolved measurements an excitation wavelength of 535 nm (and not 550 nm which corresponds to the absorption maximum of TAMRA) was used in order

to avoid overlap of the Raman scattering peak with the Chl *a* fluorescence. For the labeled complex $35 \pm 5\%$ of the absorption at 535 nm is due to TAMRA, whereas $65 \pm 5\%$ is due to Chl *b* and Chl *a*. Therefore, in the steady-state and time-resolved fluorescence measurements it can be expected that at least 65% of the Chl fluorescence is due to directly excited Chl molecules.

3.2. Steady-state fluorescence emission

The fluorescence emission spectra of CP29-WT and CP29-4 after excitation at 535 nm are shown in Fig. 2B. For CP29-4 some fluorescence can be discerned around 580 nm which is due to TAMRA but the majority of the fluorescence stems from Chl *a*, peaking around 680 nm. The shape of the fluorescence spectrum in the Chl Q_y region is identical for both complexes, indicating that the TAMRA fluorescence is negligible around 680 nm. However, there is a clear increase of the Chl *a* fluorescence intensity for CP29-4, which must be ascribed to excitation energy transfer from TAMRA to Chl *a* and *b*. It should be noted that around 100% energy transfer from Chl *b* to Chl *a* occurs on a time scale of hundreds of femtoseconds to several picoseconds [13,14,17] and therefore, Chl *b* fluorescence is virtually absent from the steady-state emission spectrum. The increase of Chl *a* fluorescence is substantially larger than the amount of TAMRA fluorescence around 580 nm, indicating that a large fraction of the excitations that are created on TAMRA has been transferred. At 535 nm the amount of directly excited Chl was estimated to be around $65 \pm 5\%$ whereas comparison of the intensities of the two fluorescence spectra at 680 nm indicates that approximately 75% of the fluorescence is due to directly excited Chl. This confirms that FRET from TAMRA to Chl is substantial but not “perfect”, i.e. less than 100%.

3.3. Steady-state fluorescence excitation spectra

The fluorescence excitation spectra of CP29-WT and CP29-4 upon detection at 680 nm are given in Fig. 2B. At 680 nm Chl fluorescence is detected selectively. The labeled complex shows a shoulder at 550 nm, which can be ascribed to TAMRA that is transferring excitation energy to Chl. Exact quantification of the energy transfer is complicated by the Raman scatter contribution upon excitation at 550 nm, which may not have been completely removed with background subtraction. The emission spectra indicate a transfer efficiency of $\sim 80\%$. From the steady-state spectra it cannot be determined whether in all complexes the transfer efficiency is 80% or whether there is heterogeneity in the efficiencies. In order to resolve this issue, time-resolved fluorescence measurements were performed.

3.4. Time-resolved streak-camera fluorescence measurements

In Fig. 3A the time-resolved fluorescence at 585 nm (TAMRA) is shown for CP29-4 and CP29 apoprotein which was labeled at the 4 position (apo-4). The apoprotein shows a decay of hundreds of picoseconds. This is faster than the 3.2 ns of TAMRA in methanol (Table 1). So TAMRA, bound to apo-4 is quenched, presumably by the protein environment (because the protein does not contain pigments, quenching due to FRET can not occur). Fluorescence quenching by a protein environment has been reported before for TAMRA and similar dyes [41,42]. CP29-4 shows much faster decay than apo-4, which must be due to FRET to the Chls. The time-resolved fluorescence of Chl *a* at 680 nm is shown in Fig. 3A; a substantial amount of fluorescence arises from direct Chl excitation. Also a rise component can be observed on a time scale of several tens of picoseconds, which is due to FRET from TAMRA to Chl.

Fig. 4 shows the result of a global analysis of the fluorescence kinetics. The fluorescence of apo-4 decays mono-exponentially

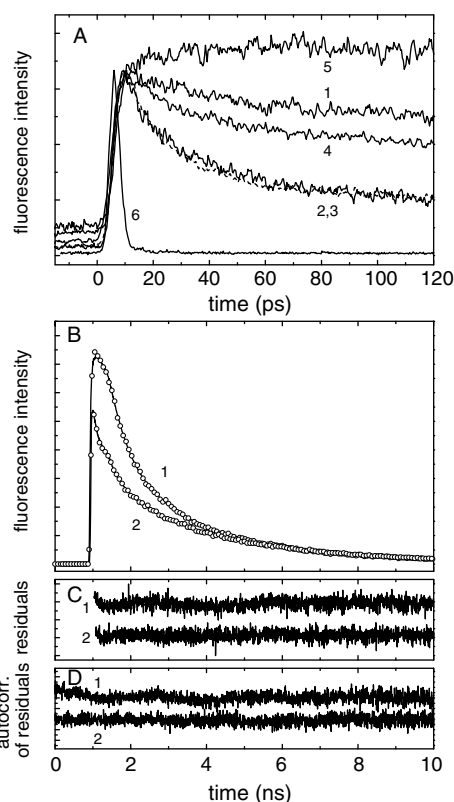


Fig. 3. Time-resolved fluorescence kinetics. (A) Measured by streak camera (averaged over 565–605 nm, excited at 535 nm): apo-4 (1), CP29-4 (2, solid), CP29-97 (3, dashed), CP29-40 (4) and a trace of mutant CP29-4 averaged over 665–705 nm (5). Curve 6 represents the excitation pulse. (B) Measured by TCSPC (detected at 585 nm, excited at 540 nm): experimental curves (markers for every 15th data point) and fitted curves (lines) of apo-4 (1) and CP29-4 (2), scaled differently for presentation purposes. (C) Residuals of the fits. (D) Autocorrelation of the residuals. C and D have offsets for presentation purpose.

Table 1

Results of fitting TCSPC fluorescence decay curves of TAMRA in methanol (MeOH), attached to the apoproteins, and attached to holoproteins: Fluorescence lifetimes (τ) and relative amplitudes (between square brackets).

	MeOH	apo-4	CP29-4	CP29-40	CP29-97
τ_1 (ns)	3.2 [1]	0.34 [0.54]	0.020 [0.76]	0.078 [0.37]	0.019 [0.77]
τ_2 (ns)	— ^a	1.46 [0.32]	0.204 [0.12]	0.323 [0.22]	0.206 [0.09]
τ_3 (ns)	— ^a	3.81 [0.14]	1.39 [0.05]	1.35 [0.24]	1.49 [0.06]
τ_4 (ns)	— ^a	— ^a	3.81 [0.07]	3.48 [0.17]	3.92 [0.09]

^a Not observed.

with a decay time of ~ 360 ps (note that time window in this experiment is only 200 ps, TCSPC measurements below show the presence of some additional slow components with small amplitudes). The data of the reconstituted, labeled mutants were each globally fitted with two time constants. In the TAMRA region the spectrum of CP29-4 shows a decrease in intensity with a time constant of 19 ps and a concomitant rise is observed in the Chl *a* region. This can be interpreted as energy transfer from TAMRA to Chl with a time constant of 19 ps, although it should be kept in mind that there is also some contribution from protein quenching to this time constant. Thus the real transfer time (τ) depends on the observed transfer time (τ_{obs}), and on the rate of protein quenching (k_q): $\tau^{-1} = \tau_{\text{obs}}^{-1} - k_q$. However, the rate of quenching by the protein is considerably slower ($(\sim 360 \text{ ps})^{-1}$ in apo-4) than τ_{obs}^{-1} , so the real transfer time is probably only slightly slower ($\sim 5\%$) than the observed transfer time. The area of the decaying component in the TAMRA region is larger than that of the

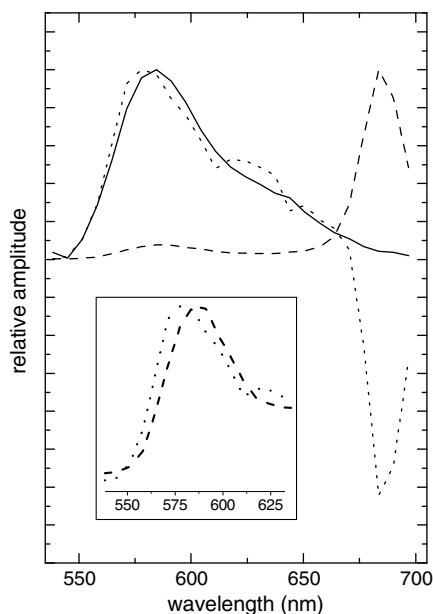


Fig. 4. Decay associated spectra (DAS) resulting from global analysis of streak images of apo-4 (solid line, $\tau = 360$ ps), and CP29-4 (dotted line, $\tau = 19$ ps [5.0]; dashed line, $\tau = 3.3$ ns [1]), normalized to the maximum. The inset shows the 19 ps [0.38] and 3.3 ns [1] components normalized to the maximum in this wavelength region. Scaling factors of each DAS are shown between square brackets.

(negative) rise component in the Chl region. This is due to some singlet–singlet annihilation of Chl excited states. Annihilation takes place when a laser pulse leads to multiple excitations within a single CP29 complex. A singlet excited state can then act as a mobile quencher for other singlet excited states in the same complex, resulting in an additional fluorescence decay component. At the applied light intensities (approximately 10 mW, lower intensities gave a too weak signal) some annihilation takes place. Annihilation in CP29 is expected to result in a decay component of tens of picoseconds [43], which is close to the observed energy transfer time. Therefore annihilation may partly mask the amplitude of the rise of Chl fluorescence due to FRET. However, the transfer time is almost identical to the one measured by TCSPC in the absence of annihilation (see below). Therefore, annihilation appears to have a relatively small effect on the observed transfer time. The second spectrum in Fig. 4 decays with a time constant of 3.3 ns, reflecting the “normal” excited-state decay of TAMRA and Chl *a*. There are several additional points to be noticed. (1) A fraction of the TAMRA molecules is not transferring its energy ($\sim 15\%$). This is in rather good agreement with the transfer efficiency estimated from the steady-state fluorescence measurements. Apparently, there is some structural heterogeneity and different conformations are present. (2) The fluorescence spectrum of the non-transferring (slowly decaying) TAMRA molecules is red-shifted with respect to that of the transferring molecules (see inset in Fig. 4), indicating that the non-transferring molecules are relatively far away from the Chl molecules and are in a more hydrophilic environment. Alternatively, the red-shift can be caused by slow solvent relaxation that can only occur in the absence of fast excitation transfer. (3) A fit with only two components represents an oversimplification of the real situation (see also below) but clearly demonstrates that a large fraction of the excitations are transferred with a time constant of ~ 20 ps.

3.5. Time-correlated single photon counting measurements

Time-resolved measurements of CP29-4 were also performed with the TCSPC technique, which offers higher S/N but lower time

resolution. Upon detection at 585 nm decay times of 20 ps (76%), 204 ps (12%), 1.39 ns (5%) and 3.81 ns (7%) were obtained (see also Fig. 3B and Table 1). The first component is in good agreement with the streak-camera results, which confirms that a large fraction of the excitations is rapidly transferred to the Chl molecules. Possibly also the 204 ps and 1.39 ns time constants correspond to energy transfer to the Chls but there is no unambiguous proof for that because similar rise times are not observed in the Chl region. Alternatively, these decay processes might be due to direct quenching of TAMRA (see above). When TAMRA is measured in apo-4, the decay times are 336 ps (54%), 1.46 ns (32%) and 3.81 ns (14%). It is interesting to note that the 336 ps decay time is close to the 360 ps that was obtained from a global analysis fit of the streak-camera data.

The fluorescence anisotropy of TAMRA in CP29-4 was determined using the TCSPC setup and is given in Fig. 5. The anisotropy was analyzed by global fitting of the parallelly and perpendicularly polarized fluorescence decay curves, as described in Section 2. Anisotropy correlation times of 550 ps (with amplitude 0.07) and 7 ns (with amplitude 0.03) and a residual anisotropy value of 0.24 (Table 3) were obtained. It should be noted that the polarized fluorescence decay curves are fitted in a non-associative way, i.e. there is no correlation assumed between the isotropic decay times and the anisotropy correlation times. Although this is not necessarily the case, associative fitting does not lead to meaningful results. However, the observed correlation times are so slow that they cannot originate from TAMRA molecules that transfer to Chl, because fluorescence of those molecules disappears in tens of picoseconds, and therefore hardly contributes to the anisotropy decay. So the observed anisotropy correlation times and the residual anisotropy originate from non-transferring TAMRA molecules, which demonstrates that the rotational motion of these molecules is strongly restricted. This indicates that the N-terminus for this subset of conformations adopts a rather static structure. No conclusion can be drawn about the dynamics in the case of fast energy transfer.

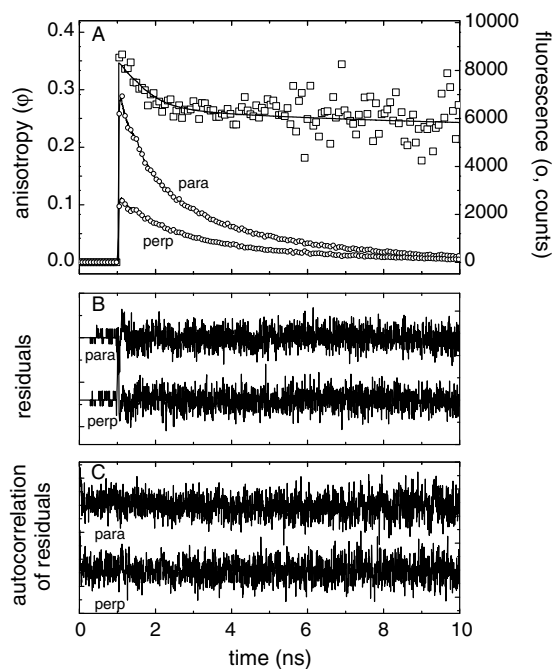


Fig. 5. Fluorescence anisotropy kinetics measured by TCSPC (detected at 585 nm, excited at 540 nm). (A) Anisotropy decay curve (squares) and decay curves of parallelly (para) and perpendicularly (perp) polarized fluorescence (markers for every 15th point) and fitted curves (lines) of CP29-4. (B) Residuals of the global fit of the polarized fluorescence decay curves. (C) Autocorrelation of the residuals. B and C have offsets for presentation purpose.

Table 2

Results of global fitting of fluorescence decay curves recorded between 540 and 700 nm, measured with the streak-camera setup: Fluorescence lifetimes (τ) and relative areas under the DAS of TAMRA attached to apo-4 and holoproteins.

	apo-4	CP29-4	CP29-40	CP29-97
τ_1 (ns)	0.36 [1]	0.019 [0.73]	0.029 [0.42]	0.019 [0.76]
τ_2 (ns)	– ^a	3.3 [0.27]	3.3 [0.58]	3.6 [0.24]

^a Not observed.

Table 3

Results of fitting TCSPC anisotropy decays of TAMRA in methanol and bound to the reconstituted mutants: Anisotropy correlation times (ϕ), with amplitudes in square brackets, and residual anisotropy (β_{inf}).

	Methanol	CP29-4	CP29-40	CP29-97
ϕ_1 (ns)	0.16 [0.34]	0.55 [0.07]	0.80 [0.04]	0.48 [0.04]
ϕ_2 (ns)	– ^a	7.0 [0.03]	4.2 [0.02]	11 [0.07]
β_{inf}	0.00	0.24	0.26	0.23

^a Not observed.

3.6. Labeled CP29 mutants 97 and 40

The results of time-resolved streak-camera measurements on labeled CP29-97 are very similar to those obtained for labeled CP29-4 (Fig. 3A and Table 2). Global analysis with two components leads to lifetimes of 18.6 ps (transfer) and 3.6 ns (overall excited-state decay). TCSPC data of CP29-97 show four decay components in the TAMRA fluorescence region: 19 ps (77%), 206 ps (9%), 1.49 ns (6%) and 3.92 ns (9%) (see Table 1). The anisotropy data reveal two correlations times of 479 ps (amplitude 0.04) and 11 ns (amplitude 0.07) and a residual anisotropy of 0.23 (see Table 3). These results are again similar to those of CP29-4.

Fig. 3A also shows the fluorescence decay of TAMRA in CP29-40. In this case the decay resembles mostly that of the non-transferring apo-4. Global analysis with two components reveals a lifetime of 29 ps but its amplitude is only 40%, probably largely due to protein quenching (see Table 2). No rise could be detected in the Chl region suggesting absence of energy transfer although it can not be excluded that singlet–singlet annihilation is masking a small rise. TCSPC data of CP29-40 show four decay components in the TAMRA fluorescence region: 78 ps (37%), 323 ps (22%), 1.35 ns (24%) and 3.48 ns (17%) (see Table 1). No rise could be detected in the Chl region. The anisotropy data reveal two correlations times of 797 ps (amplitude 0.04) and 4.2 ns (amplitude 0.02) and a residual anisotropy of 0.26 (see Table 3). These values are similar to those of CP29-4.

4. Discussion

The presented fluorescence kinetics data reveal fast (tens of ps) excitation energy transfer in some cases, possibly some transfer in the hundreds of ps but also some TAMRA molecules that do not or hardly show any energy transfer. In order to interpret the meaning of these observations it is important to apply the Förster equation [44]: $\tau/\tau_F = (R/R_0)^6$, where R_0 is the Förster radius, R is the center-to-center distance between donor and acceptor, τ equals the inverse of the energy transfer rate from a donor molecule (TAMRA) to an acceptor molecule (Chl *a*) and τ_F is the fluorescence lifetime of the donor (3.2 ns in methanol, see Table 1) and was measured in the solvent that was used for calculating the fluorescence quantum yield. The latter is needed for the calculation of the Förster radius, which is defined as

$$R_0 = 0.211 * [\kappa^2 * n^{-4} * Q_D * J(\lambda)]^{1/6},$$

where κ is the orientation factor, n the refractive index (its exact meaning in this equation is extensively discussed in [45]), Q_D is the quantum yield of the donor in absence of acceptor, and $J(\lambda)$ is the overlap integral of the fluorescence emission spectrum of the donor and the absorption spectrum of the acceptor. R_0 was calculated with $\kappa^2 = 2/3$, $n = 1.4$ (a value typical for a dye, between $n \approx 1.33$ of buffer and $n \approx 1.5$ of proteins [46]), $Q_D = 0.66$ (MTS-TAMRA measured in methanol, using as a reference TAMRA (Invitrogen) in methanol, with a reported value of $Q_D = 0.68$). $J(\lambda)$ was calculated from the absorption spectrum of Chl *a* in a protein environment [47] (scaling extinction coefficient of the red-most peak to $8630 \text{ m}^2 \text{ mol}^{-1}$ [48]) and the emission spectrum of TAMRA in DM buffer. The absorption spectrum of Chl *a* was used, instead of Chl *b*, for the following reasons: Chl *a* is probably closer to TAMRA than Chl *b* (see Fig. 1), CP29 contains 3 times more Chl *a* than Chl *b*, and the spectra of Chl *a* and *b* are very similar in the region of TAMRA emission. This leads to a value of $R_0 = 5.0 \text{ nm}$. The rate of transfer is very sensitive to the distance between the chromophores and for instance a transfer time of 10 ps corresponds to a distance of 1.9 nm whereas a time of 300 ps corresponds to 3.4 nm. It should be kept in mind that in the case of CP29 there are several potential acceptors available and the observed transfer rate is simply the sum of the individual transfer rates to the various Chls. Note that an uncertainty in the transfer rate of 5% (see Section 3) leads to an uncertainty in the distance R which is smaller than 1% because the transfer rate is proportional to R^{-6} .

In the case of CP29-4, a large fraction of the excitations (around 80%) is transferred to the Chls with a rate of $(20 \text{ ps})^{-1}$, indicating that the distance to one or more of the Chls is of the order of 2 nm. If the secondary structure of the N-terminus would be an α -helix, the distance from amino acid 4 and 105 (which is near the beginning of the Chl-containing part of the protein) would be around 15 nm (with a calculated transfer time of $\sim 2 \mu\text{s}$). Therefore, it is immediately clear that in approximately 80% of the complexes, the end of the N-terminal loop is folded back to the hydrophobic part of the protein. It is however unclear as to why in the remaining 20% of the cases no energy transfer is observed. One straightforward explanation is that in these cases the loop is not folded back. However, the observed kinetics for CP29-97 is nearly identical to that of CP29-4 and in that case it is more difficult to imagine how TAMRA bound to residue 97, which is close to the transmembrane region, can be far away from the Chls. The latter observations suggest that detailed structural modeling would be needed to investigate this possibility. Whatever the exact reason may be, it is clear that TAMRA is in a rather rigid environment when it is not transferring its excitations in CP29-4 and CP29-97 as can be concluded from the slow anisotropy correlation times and the large value of the residual anisotropy. The energy transfer from TAMRA bound at position 40 is clearly less efficient than that from the other reconstituted samples, leading to the conclusion that residue 40 is farther away from the Chls. Position 40 is close to the region which, based on the primary structure, was suggested to bind one of the central carotenoids [5], indicating its proximity to the transmembrane domain. However, this region later turned out not to be involved in carotenoid binding [6], which is in agreement with the reduced amount of energy transfer from the label at position 40 to Chl.

In conclusion, it turned out to be possible to attach a chromophore with high efficiency at a specific position in the N-terminal domain of CP29 and to measure the ultrafast energy transfer from this label to the Chls. This opens up the possibility to probe the entire N-terminal loop and determine distances and heterogeneity and also local mobility/flexibility when the energy transfer is not very efficient. These first measurements indicate qualitatively that the end of the N-terminus is folded back on the hydrophobic part of the protein but they also show that there is some structural

heterogeneity. Further experiments and data analysis combined with structural calculations are in progress, and may yield more quantitative results.

Acknowledgements

This work is part of the research program of the “Stichting voor Fundamenteel Onderzoek der Materie (FOM)”, which is financially supported by the “Nederlandse Organisatie voor Wetenschappelijk Onderzoek (NWO)”. B.v.O. was supported by FOM. RC acknowledges support (visitor grant) from the “Nederlandse Organisatie voor Wetenschappelijk Onderzoek (NWO)”. SM gratefully acknowledges the graduate school Experimental Plant Sciences for financial support.

The authors thank Ivo H.M. van Stokkum (Vrije Universiteit Amsterdam, the Netherlands) for help with data analysis.

References

- [1] E.J. Boekema, H. van Roon, J.F.L. van Breemen, J.P. Dekker, *Eur. J. Biochem.* 266 (1999) 444.
- [2] T.K. Ahn, T.J. Avenson, M. Ballottari, Y.-C. Cheng, K.K. Niyogi, R. Bassi, G.R. Fleming, *Science* 320 (2008) 794.
- [3] T.J. Avenson, T.K. Ahn, D. Zigmantas, K.K. Niyogi, Z. Li, M. Ballottari, R. Bassi, G.R. Fleming, *J. Biol. Chem.* 283 (2008) 3550.
- [4] M. Mozzo, F. Passarini, R. Bassi, H. van Amerongen, R. Croce, *Biochim. Biophys. Acta* 1777 (2008) 1263.
- [5] R. Bassi, R. Croce, D. Cugini, D. Sandona, *Proc. Natl. Acad. Sci. USA* 96 (1999) 10056.
- [6] M. Gastaldelli, G. Canino, R. Croce, R. Bassi, *J. Biol. Chem.* 278 (2003) 19190.
- [7] S. Caffarri, F. Passarini, R. Bassi, R. Croce, *FEBS Lett.* 581 (2007) 4704.
- [8] R. Simonetto, M. Crimi, D. Sandona, R. Croce, G. Cinque, J. Breton, R. Bassi, *Biochemistry* 38 (1999) 12974.
- [9] D. Leupold, K. Teuchner, J. Ehlert, K.-D. Irrgang, G. Renger, H. Lokstein, *J. Biol. Chem.* 281 (2006) 25381.
- [10] M. Ratsep, J. Pieper, K.D. Irrgang, A. Freiberg, *J. Phys. Chem. B* 112 (2008) 110.
- [11] J. Pieper, K.D. Irrgang, M. Ratsep, J. Voigt, G. Renger, G.J. Small, *Photochem. Photobiol.* 71 (2000) 574.
- [12] A. Pascal, C. Gradinaru, U. Wacker, E. Peterman, F. Calkoen, K.-D. Irrgang, P. Horton, G. Renger, R. van Grondelle, B. Robert, H. van Amerongen, *Eur. J. Biochem.* 262 (1999) 817.
- [13] J.M. Salverda, M. Vengris, B.P. Krueger, G.D. Scholes, A.R. Czarnoleski, V.I. Novoderezhkin, H. van Amerongen, R. van Grondelle, *Biophys. J.* 84 (2003) 450.
- [14] R. Croce, M.G. Müller, R. Bassi, A.R. Holzwarth, *Biophys. J.* 84 (2003) 2508.
- [15] R. Croce, M.G. Müller, S. Caffarri, R. Bassi, A.R. Holzwarth, *Biophys. J.* 84 (2003) 2517.
- [16] G. Cinque, R. Croce, A. Holzwarth, R. Bassi, *Biophys. J.* 79 (2000) 1706.
- [17] C.C. Gradinaru, I.H.M. van Stokkum, A.A. Pascal, R. van Grondelle, H. van Amerongen, *J. Phys. Chem. B* 104 (2000) 9330.
- [18] C.C. Gradinaru, A.A. Pascal, F. van Mourik, B. Robert, P. Horton, R. van Grondelle, H. van Amerongen, *Biochemistry* 37 (1998) 1143.
- [19] M.G. Testi, R. Croce, P. Polverino-De Laureto, R. Bassi, *FEBS Lett.* 399 (1996) 245.
- [20] E. Bergantino, D. Sandonà, D. Cugini, R. Bassi, *Plant Mol. Biol.* 36 (1998) 11.
- [21] S. Mauro, P. Dainese, R. Lannoye, R. Bassi, *Plant Physiol.* 115 (1997) 171.
- [22] R. Croce, J. Breton, R. Bassi, *Biochemistry* 35 (1996) 11142.
- [23] M. Hansson, A.V. Vener, *Mol. Cell. Proteomics* 2 (2003) 550.
- [24] J. Standfuss, A.C. Terwisscha van Scheltinga, M. Lamborghini, W. Kühlbrandt, *EMBO J.* 24 (2005) 919.
- [25] Z.F. Liu, H. Yan, K. Wang, T. Kuang, J. Zhang, L. Gui, W. Chang, *Nature* 428 (2004) 287.
- [26] R. Horn, H. Paulsen, *J. Biol. Chem.* 279 (2004) 44400.
- [27] K. Nagai, H.C. Thøgersen, *Methods Enzymol.* 153 (1987) 461.
- [28] H. Paulsen, U. Rüdiger, *Planta* 181 (1990) 204.
- [29] R.J. Porra, W.A. Thompson, P.E. Kriedemann, *Biochim. Biophys. Acta* 975 (1989) 384.
- [30] B.H. Davies, in: T.W. Goodwin (Ed.), *Chemistry and Biochemistry of Plant Pigments*, Academic Press, New York, 1965, pp. 489–532.
- [31] R.B. Spruijt, A.B. Meijer, C.J.A.M. Wolfs, M.A. Hemminga, *Biochim. Biophys. Acta* 1509 (2000) 311.
- [32] I.H.M. van Stokkum, B. van Oort, F. van Mourik, B. Gobets, H. van Amerongen, in: T.J. Aartsma, J. Matysik (Eds.), *Biophysical Techniques in Photosynthesis*, vol. 2, Springer, Dordrecht, 2008, pp. 223–240.
- [33] I.H.M. van Stokkum, D.S. Larsen, R. van Grondelle, *Biochim. Biophys. Acta* 1657 (2004) 82.
- [34] J.W. Borst, M.A. Hink, A. van Hoek, A.J.W.G. Visser, *J. Fluoresc.* 15 (2005) 153.
- [35] A. van Hoek, A.J.W.G. Visser, *Anal. Instrum.* 14 (1985) 359.
- [36] H.-J. Lin, H. Szmecinski, J.R. Lakowicz, *Anal. Biochem.* 269 (1999) 162.
- [37] B. van Oort, A. Amunts, J.W. Borst, A. van Hoek, N. Nelson, H. van Amerongen, R. Croce, *Biophys. J.* (2008), doi:10.1529/biophysj.108.140467.
- [38] A. van Hoek, K. Vos, A.J.W.G. Visser, *IEEE J. Quantum Electron.* QE-23 (1987) 1812.
- [39] A.V. Digris, V.V. Skakoun, E.G. Novikov, A. van Hoek, A. Claiborne, A.J.W.G. Visser, *Eur. Biophys. J.* 28 (1999) 526.
- [40] N.V. Visser, W.G. Westphal, A. van Hoek, C.P.M. van Mierlo, A.J.W.G. Visser, H. van Amerongen, *Biophys. J.* 95 (2008) 2462.
- [41] A. Cha, F. Bezanilla, *J. Gen. Physiol.* 112 (1998) 391.
- [42] N. Marmé, J.P. Knemeyer, M. Sauer, J. Wolfrum, *Bioconjug. Chem.* 14 (2003) 1133.
- [43] V. Barzda, V. Gulbinas, R. Kananavicius, V. Cervinskaskas, H. van Amerongen, R. van Grondelle, L. Valkunas, *Biophys. J.* 80 (2001) 2409.
- [44] T. Förster, *Z. Naturforsch.* 4a (1949) 321.
- [45] R.S. Knox, H. van Amerongen, *J. Phys. Chem. B* 106 (2002) 5289.
- [46] J.R. Lakowicz, *Principles of Fluorescence Spectroscopy*, vol. 1, New York, 1999.
- [47] R. Croce, G. Cinque, A.R. Holzwarth, R. Bassi, *Photosynth. Res.* 64 (2000) 221.
- [48] H.H. Strain, M.R. Thomas, J.J. Katz, *Biochim. Biophys. Acta* 75 (1963) 306.